JACS
JOURNAL OF THE AMERICAN CHEMICAL SOCIETY

Article

pubs.acs.org/JACS

Direct *In situ* Observation of Li_2O Evolution on Li-Rich High-Capacity Cathode Material, $Li[Ni_xLi_{(1-2x)/3}Mn_{(2-x)/3}]O_2$ $(0 \leq x \leq 0.5)$

Sunny Hy,[†] Felix Felix,[†] John Rick,[†] Wei-Nien Su,[†] and Bing Joe Hwang*[,†,‡]

[†]Nanoelectrochemistry laboratory, Department of Chemical Engineering, National Taiwan University of Science and Technology, Taipei, Taiwan 10607

[‡]National Synchrotron Radiation Research Center, Hsin-Chu, Taiwan 30076

Supporting Information

ABSTRACT: High-capacity layered, lithium-rich oxide cathodes show great promise for use as positive electrode materials for rechargeable lithium ion batteries. Understanding the effects of oxygen activating reactions on the cathode's surface during electrochemical cycling can lead to improvements in stability and performance. We used *in situ* surfaced-enhanced Raman spectroscopy (SERS) to observe the oxygen-related surface reactions that occur during electrochemical cycling on lithium-rich cathodes. Here, we demonstrate the direct observation of Li_2O formation during the extended plateau and discuss the consequences of its formation on the cathode and anode. The formation of Li_2O on the cathode leads to the formation of species related to the generation of H_2O together with LiOH and to changes within the electrolyte, which eventually result in diminished performance. Protection from, or mitigation of, such devastating surface reactions on both electrodes will be necessary to help realize the potential of high-capacity cathode materials (270 $mAhg^{-1}$ versus 140 $mAhg^{-1}$ for $LiCoO_2$) for practical applications.

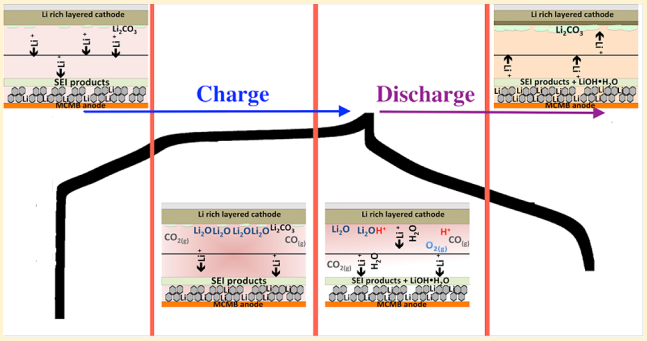

INTRODUCTION

Lithium-rich cathode materials, represented in solid solution notation as $Li[Ni_xLi_{(1-2x)/3}Mn_{(2-x)/3}]O_2$ $(0 \leq x \leq 0.5)$[1] or in composite notation as $xLi_2MnO_3 \cdot (1-x)LiMn_{0.5}Ni_{0.5}O_2$[2,3] (LLNMO), have generated a large amount of interest over the past decade due to their high reversible capacities (>270 mAh/g).[4−8] Ohzuku et al.[9] demonstrated that the capacity can reach 300 or even 350 mAh/g using slower rates or higher temperatures, respectively.[9] However, the charging mechanism is still uncertain,[7,10] while additionally the surface structural changes that lead to capacity fade and instability remain unresolved. Ito et al.[11] showed that there is continuous formation of Li_2CO_3 on the cathode's surface with subsequent decomposition as the result of oxygen reduction during discharge below 3.0 V. Similarly, Hong et al.[12] performed *ex situ* FTIR and showed Li_2CO_3 formation and subsequent decomposition upon discharging and charging, which they described as being attributable to the involvement of oxygen radicals. Lu et al.[5] first proposed the extraction of Li_2O from LLNMO, during the plateau region with the simultaneous extraction of Li and O, to explain its anomalously high capacity. However, Li_2O has not been directly observed in this region and has only been tentatively observed in the discharged state by *ex situ* time-of-flight secondary ion mass spectroscopy, where Li_2O^+ and LiC_2^+ were observed and may be generated from not only Li_2O but also from LiO_2, Li_2O_2, Li_2CO_3, etc.[11] Due to the sensitive nature of the electrode and electrolyte interface, direct observation of surface species during electrochemical cycling would help to clarify the involvement of oxygen. Previous reports have made use of surface enhanced Raman spectroscopy (SERS) to observe the oxygen-related reactions that occur in a nonaqueous Li^+ electrolyte system on a Au electrode.[13] Generally, any surface species formation is only observable through the use of SERS-active substrates and not in an actual working electrode due to the thin and small nature of the surface formed. Here we demonstrate the application of SiO_2-coated Au nanoparticles that utilize SERS signal enhancement on an LLNMO electrode to study the formation of surface species during electrochemical cycling. While bare Au nanoparticles are not anticipated to participate or dramatically affect the overall system, the insulating and inert SiO_2 coating insures the isolation of the Au nanoparticle from the probed material and avoids the special affinity associated with certain species that may adsorb on to the nanoparticle. This SiO_2 coating also serves to avoid the agglomeration of the nanoparticles that may reduce signal enhancement.[14] We show the ability of this technique to directly observe Li_2O species formation during charging and discuss the reactions that lead to its formation and consumption. By combining previous observations with this study's findings, we attempt to show the existence of the different species formed at various stages of cycling and the

Received: October 2, 2013
Published: December 23, 2013

   dx.doi.org/10.1021/ja410137s | J. Am. Chem. Soc. 2014, 136, 999−1007

formation of Li_2O, based on the participation of the anion and thus link the different reactions that lead to changes within the entire battery, including the cathode, anode, and electrolyte.

EXPERIMENTAL SECTION

Raw Materials. Li_2O, Li_2O_2, and $MnCO_3$ were purchased from Sigma Aldrich; Li_2CO_3, $LiOH{\cdot}H_2O$, $Mn(SO_4){\cdot}H_2O$, and $Ni(SO_4){\cdot}H_2O$ were purchased from Acros Organics; and Na_2CO_3 and NH_4OH were purchased from J.T. Baker without modification or treatment. Li_2O was stored in an Ar-filled glovebox with <1 ppm O_2 or H_2O before analysis.

Synthesis of the Lithium-Rich Cathode LLNMO. $Li_{1.2}Ni_{0.2}Mn_{0.6}O_2$ (x = 0.2) and $LiNi_{0.5}Mn_{0.5}O_2$ (x = 0.5) were synthesized by a carbonate coprecipitation. Transition-metal sulfates and Na_2CO_3 were separately dissolved in DI water. The mixed-metal sulfate solution was slowly dripped into the Na_2CO_3 solution. After stirring for 10 h the solution was vacuum-filtered, washed with DI water, and dried overnight in a vacuum oven. The resulting precipitates were mixed with Li_2CO_3, fired at 900 °C for 12 h, and then quenched to room temperature. The Li_2MnO_3 (x = 0) was synthesized by grinding $MnCO_3$ and Li_2CO_3 in a Fritsch planetary ball mill for 1 h at 150 rpm and then annealing at 400 °C for 32 h.[15]

Characterization. X-ray powder diffraction (XRD) was performed on a Bruker D2 phaser diffractometer equipped with a Cu Kα radiation source and a lynxeye detector. The surface morphologies and particle sizes of the synthesized powders were examined using scanning electron microscopy (JEOL, JSM 6500). Raman microspectroscopy measurements were performed on a ProMaker system mounted with one TE cooled CCD (1024 × 256 pixels) integrated by Protrustech Corporation Limited. The system was equipped with a 50× long working distance lens (Olympus America inc.) operated with an excitation wavelength of 532 nm, with ∼1 mW laser power, unless specified, to avoid degradation to the standards or electrodes.[16] The exposure time was 10 s with 10 accumulations. Calibration was done using a silicon standard where the band is generally observed at 520 cm^{-1}. Raman analysis of Li_2O, Li_2O_2, and $LiOH{\cdot}H_2O$ was undertaken by placing the sample in a sealed holder with a 0.17 mm thick quartz window prepared within in the Ar-filled glovebox.

Electrode Fabrication. The lithium-rich cathode was fabricated by mixing the cathode powder, Super P carbon, and polyvinylidene fluoride (PVdF) (weight ratio 80:10:10) to form a slurry using *N*-methyl-2-pyrrolidone (NMP). The slurry was cast over an Al foil which was then dried in a vacuum oven overnight. A graphite anode was fabricated by mixing mesocarbon microbeads (MCMB-2528, Osaka Gas), Super P conductive carbon, PVdF binder (weight ratio 90:7:3) to form a slurry using NMP. The slurry was cast over a Cu foil, which was then dried in a vacuum oven overnight.

Electrochemical Measurements. A commercial electrolyte comprising ethylene carbonate/diethyl carbonate (EC/DEC) 1:1 with added $LiPF_6$ (1 M) was used in a half-cell 2032 coin cell-type battery with a Li foil counter electrode. Cyclic voltammetry (CV) measurements were made using an Autolab potentiostat running at 0.1 mV/s from the open circuit potential to 5 V and then back to 2 V. The charge and discharge measurements were run galvanostatically at 0.1 C (C = 250 mAh/g) from 2.0–4.8 V.

***In situ* SERS.** Au nanoparticles (NPs) 30–40 nm in diameter with a SiO_2 coating (3–4 nm) were synthesized as in previous reports with some modifications.[17] Briefly, (3-aminopropyl) trimethoxysilane (1 mM) was added to the sol under vigorous magnetic stirring, followed by the addition of a 0.54 wt % sodium silicate solution. The washed and dried Au@SiO_2 NPs were transferred to an Ar-filled glovebox and redispersed in diethyl carbonate (DEC). The NPs were dripped onto the electrode surface and dried allowing the coin cell to be assembled. A small hole was drilled in the top cap and stainless steel disk. A small hole was also made in the lithium foil and separator in order to observe the cathode's surface. After the coin cell was assembled, a 0.17 mm thick quartz window was applied to the top cap. All procedures were undertaken in an Ar-filled glovebox with O_2 and H_2O levels maintained at <1 ppm. CV was performed at 1 mV/s from 2 to 4.8 V where the voltage was held before and during each acquisition.

Raman Mapping. The *in situ* SERS cathode electrodes were extracted from the coin cell battery, washed with DEC, and placed within a sealed holder. Spectral images were taken over a 100 × 100 μm area with 5 μm/point scan step with a 1 μm spatial resolution.

RESULTS

Raman, XRD, and SEM Characterization. SEM measurements with LLNMO x = 0, 0.2, and 0.5 can be seen in Figure 1a–c. Although Li_2MnO_3 was synthesized using a solid-state

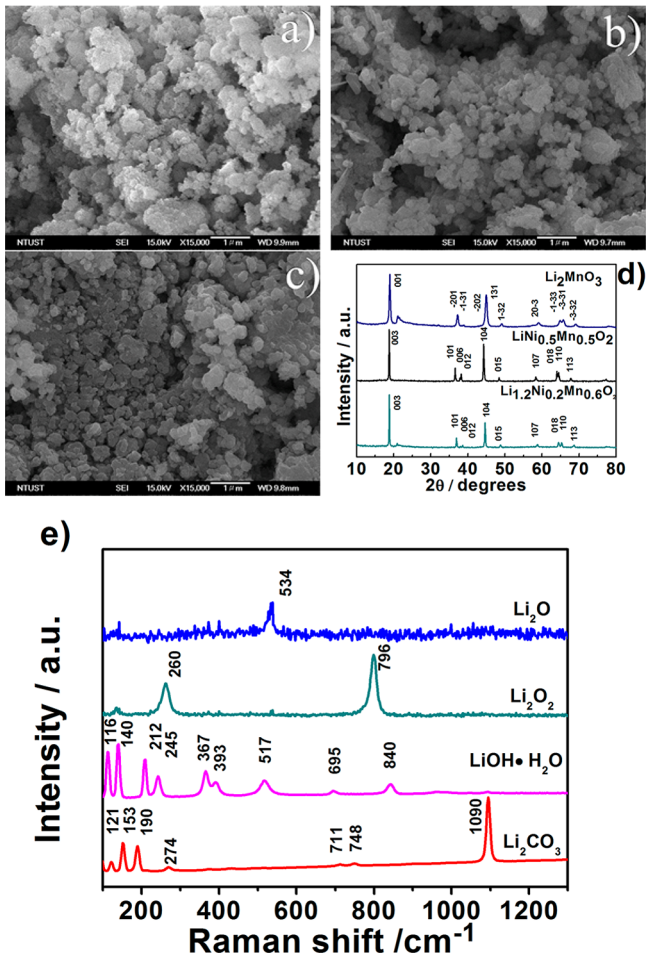

Figure 1. SEM images of: (a) Li_2MnO_3, (b) $LiNi_{0.5}Mn_{0.5}O_2$, and (c) $Li_{1.2}Ni_{0.2}Mn_{0.6}O_2$; (d) shows XRD patterns for the three samples, while (e) shows the Raman spectra of the different standards.

method, all the samples have similar morphologies and particle sizes ranging from 100 to 300 nm. XRD profiles are shown in Figure 1d. The samples $Li_{1.2}Ni_{0.2}Mn_{0.6}O_2$ and $LiNi_{0.5}Mn_{0.5}O_2$ are indexed according to the parent hexagonal structure with space group $R\bar{3}m$. The superlattice peak found at 20–25° for $Li_{1.2}Ni_{0.2}Mn_{0.6}O_2$ corresponds to cation ordering within the transition-metal plane between the Ni, Li, and Mn atoms.

Li_2MnO_3 is indexed according to the conventional monoclinic cell with space group $C2/m$ where the peak around 20–25° is a superlattice peak from the ordering of the Li and Mn atoms in the transition-metal layer. For Li_2MnO_3, the superlattice peak is broad, probably due to a large amount of stacking faults in the material synthesized at low temperature. Figure 1e shows the Raman spectra of several possible surface

dx.doi.org/10.1021/ja410137s | J. Am. Chem. Soc. 2014, 136, 999–1007

species that will serve as reference compounds for comparison to the surface species formed on the electrodes during electrochemical cycling.[13,18−20] Generally, Li_2CO_3 is the most commonly observed species on both the anode and cathode surfaces.[19,21,22] $LiOH·H_2O$ has been observed in some cases but is generally considered to be due to water contamination during electrode extraction during *ex situ* measurements:[19] It should be noted that a band at 3567 cm^{-1} corresponding to the OH stretching mode is also observed for $LiOH·H_2O$ (see Figure S1).[20] Li_2O_2 and Li_2O are generally found in Li−O_2 battery systems, where *in situ* SERS utilizing a Au electrode was used to observe minute traces of the oxygen-related species that form on the surface of the electrode during electrochemical voltage steps.[13,23−25]

Electrochemical Measurements. The CV profiles (first two cycles) of Li_2MnO_3, $LiNi_{0.5}Mn_{0.5}O_2$, and $Li_{1.2}Ni_{0.2}Mn_{0.6}O_2$ are shown in Figures 2a−c. The CV profile of Li_2MnO_3 is

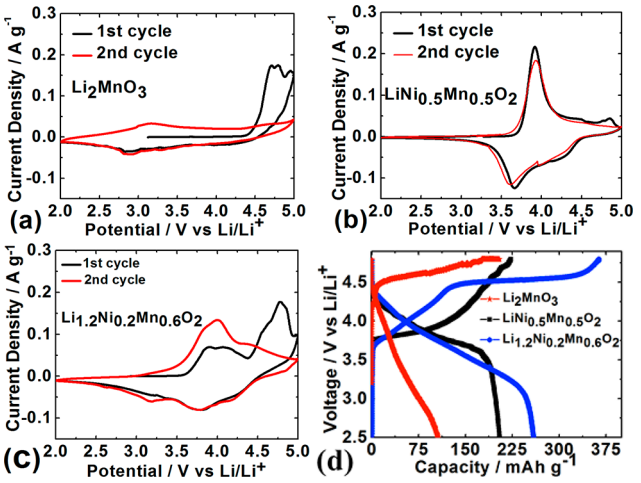

Figure 2. CV curves for the first 2 cycles of: (a) Li_2MnO_3, (b) $LiNi_{0.5}Mn_{0.5}O_2$, and (c) $Li_{1.2}Ni_{0.2}Mn_{0.6}O_2$. (d) Charge and discharge curves for the first cycle for the three members.

shown in Figure 2a where the first cycle exhibits no oxidation peak until ∼4.5 V after which the current increases steadily, due to simultaneous lithium extraction and oxygen activation. A reduction peak can be observed below 3.0 V for the first cycle corresponding to Mn^{3+} formation.[26] For the second cycle, the oxygen-activating reaction is not observed, indicating that this process is irreversible. An oxidation peak slightly above 3.0 V can be observed, together with a reduction peak below 3.0 V. These two peaks may correspond to the partial activity of the $Mn^{3+/4+}$ redox couple due to oxygen-activation reaction.[27] As shown in the CV profile of $LiNi_{0.5}Mn_{0.5}O_2$, see Figure 2b, the onset potential is ∼3.7 V for the $Ni^{2+/4+}$ redox couple and ends at 4.4 V. Unlike Li_2MnO_3, no major peak is observed for the higher voltage range, only a smaller peak at ∼4.8 V which has been observed before.[28] This may be due to a small fraction of lithium-rich structure within the $LiNi_{0.5}Mn_{0.5}O_2$ that undergoes slight oxygen activation toward the end of charging. A reduction peak is observed with the lowest value centered at ∼3.6 V which corresponds to the $Ni^{2+/4+}$ redox couple. No peak is observed below 3.0 V, indicating no Mn^{3+} formation after cycling. During the second cycle, only the $Ni^{2+/4+}$ redox pair undergoes oxidation and reduction, indicating that most of the charge compensation mechanism is due to the $Ni^{2+/4+}$ redox couple. The CV profile of $Li_{1.2}Ni_{0.2}Mn_{0.6}O_2$ is shown in Figure 2c where the onset, center, and ending potentials for the $Ni^{2+/4+}$ redox peak are observed at ∼3.7, ∼4.0, and ∼4.5 V, respectively. The subsequent oxidation peak from 4.5 to 5.0 V is similar to that representing simultaneous lithium extraction and oxygen activation, as seen in Figure 2a. During reduction, the $Ni^{2+/4+}$ redox peak at ∼3.6 V resembles $LiNi_{0.5}Mn_{0.5}O_2$, however below 3.6 V the current does not quickly decrease to zero but gradually drops in a similar manner to Li_2MnO_3. For the second cycle, unlike $LiNi_{0.5}Mn_{0.5}O_2$, the Ni redox couple does not entirely compensate for the large discharge capacity. During oxidation, the peak centered at 4.0 V shows an increase in intensity that may be due to Mn or oxygen participation. The higher voltage region does not show the oxygen-activating peak. For reduction, a smaller peak at ∼3.2 V can be observed, similar to Li_2MnO_3, indicating the presence of Mn^{3+}.[25,27] An obvious shoulder at around 4.3 V is thought to originate from the $O^{2-/-}$ redox couple.[27,29] Figure 2d shows the charge and discharge curves for the three members of LLNMO. For Li_2MnO_3, only the plateau is observed in the high-voltage region, together with a falling curve that gives a capacity of 100 mAh/g and an irreversibly capacity (IC) of over 50% during discharge. $LiNi_{0.5}Mn_{0.5}O_2$ shows the solid solution line of the $Ni^{2+/4+}$ redox couple with a corresponding discharge curve showing 200 mAh/g with only 12% IC. $Li_{1.2}Ni_{0.2}Mn_{0.6}O_2$ shows a solid solution line up to 120 mAh/g during charging, which is associated with the $Ni^{2+/4+}$ redox couple. A long plateau corresponding to oxygen activation is followed and gives an additional 250 mAh/g. Upon discharging, $Li_{1.2}Ni_{0.2}Mn_{0.6}O_2$ does not exhibit the plateau found during charging but a sloping line showing 255 mAh/g with 32% IC.

***In Situ* SERS.** Figure 3a,b shows the *in situ* SERS spectra of Li_2MnO_3 for charging and discharging, respectively. At the open circuit potential (OCV), bands are found at 504 and 620 cm^{-1}. The band at 620 cm^{-1} corresponds to the A_{1g} mode of Li_2MnO_3[30] and can be observed throughout charging. It moves to higher frequencies and returns to 620 cm^{-1} when discharged, and the lower frequency band at 504 cm^{-1} has become discernible indicating symmetry changes within the structure.[31] The 504 cm^{-1} band also shows some distortion in the oxygen-activation plateau region and also at 2.5 V, possibly due to the dramatic structural rearrangements occurring in the plateau region.[32] When charging begins, a band at 1090 cm^{-1} emerges corresponding to the CO_3 molecular unit.[33] This indicates the formation of Li_2CO_3 that has also been observed in FTIR and XPS when charged for other cathode materials[21,22]. The Li_2O band can be observed at 534 cm^{-1} when the voltage reaches close to the oxygen-activating plateau (4.4 V) and reaches its highest intensity at 4.52 V.

A sharp band at 834 cm^{-1} can also be observed starting at 4.4 V, which may correspond to the C−O stretching modes of an ester, or ether, that forms due to electrolyte degradation.[34] Jiang et al.[35] have proposed that oxidation of the electrolyte solvents forms organic species, such as aldehydes or ketones. The band may also correspond to LiOH formed from Li_2O.[36] Once the end of charging is reached (4.8 V), the band of Li_2CO_3 gradually declines. This corresponds well with the degradation of Li_2CO_3 at the charged state noted in previous studies of LLNMO.[11,12] Surprisingly, the Li_2O band also gradually disappears at the end of charging. During discharging, the 1090 cm^{-1} band of Li_2CO_3 reforms at 4.4 V and is present after discharging to 2.0 V. *In situ* SERS spectra of $LiNi_{0.5}Mn_{0.5}O_2$ for charging and discharging are shown in Figure 3c,d, respectively. The E_g and A_{1g} bands are observed at

dx.doi.org/10.1021/ja410137s | J. Am. Chem. Soc. 2014, 136, 999−1007

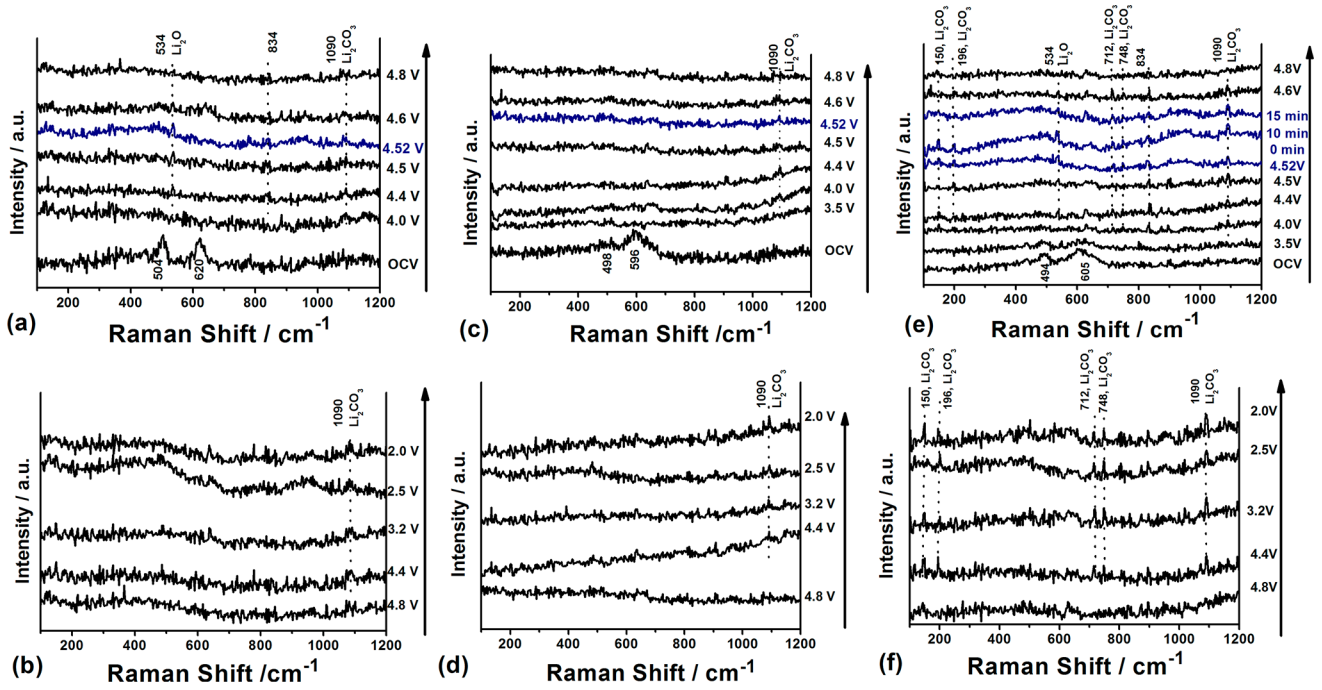

Figure 3. *In situ* SERS spectra of Li_2MnO_3 during (a) charging and (b) discharging; $LiNi_{0.5}Mn_{0.5}O_2$ during (c) charging and (d) discharging; and $Li_{1.2}Ni_{0.2}Mn_{0.6}O_2$ during (e) charging and (f) discharging. Arrows indicate voltage direction.

498 and 596 cm^{-1}, respectively. Similar to Li_2MnO_3, these bands begin to lose intensity once the voltage begins to increase together with the emergence of the band at 1090 cm^{-1} corresponding to Li_2CO_3. Throughout the first cycle, the band at 834 cm^{-1} was not observed, and no indication of Li_2O formation was apparent. Figure 3e,f shows the *in situ* SERS spectra of $Li_{1.2}Ni_{0.2}Mn_{0.6}O_2$ for charging and discharging, respectively, while the bands at 494 and 605 cm^{-1} correspond to the E_g mode and A_{1g} mode, respectively.[37] The A_{1g} mode can be seen to move to higher frequencies upon charging and shifts back to the lower frequency upon discharging. A distortion, similar to Li_2MnO_3, to the E_g band region can also be seen during the plateau region, which may also be related to the structural rearrangement.[32] When the electrode was discharged to 2.0 V, the A_{1g} and E_g modes can be observed, however the peaks are broader and the signal is much lower compared to the OCV state; this is similar to a previous *in situ* Raman spectroscopy study on the bulk changes within a similar material.[38] Unlike the current report, they did not observe surface formation where observation of Li_2CO_3 bands appear at 150, 196, 712, 748, and 1090 cm^{-1}. Similar to Li_2MnO_3, the band at 834 is observed starting at 4.0 V. The Li_2O band can be observed when the voltage reaches close to the oxygen plateau (4.4 V) and continuously increases as the voltage increases to 4.52 V. Raman spectra were acquired while the voltage was held at 4.52 V for several minutes to observe if the Li_2O band would gradually decrease similarly to Li_2MnO_3. The Li_2O band continues to increase (up to 10 min) and then subsequently decreases with increasing voltage. Possible reactions are proposed to consolidate the formation and consumption of Li_2O discussed later in this paper. Upon reaching 4.8 V, all bands dramatically decrease in intensity similar to Li_2MnO_3. When discharging toward 2.0 V, the Li_2CO_3 bands appear as early as 4.4 V. This is in good agreement with previous reports that show the consumption of Li_2CO_3 at the top of the charge (4.8 V) and reformation when discharged.[12,39] $LiNi_{0.5}Mn_{0.5}O_2$ does not exhibit the intense oxidation peak above ~4.5 V in its CV profile, which is observed with Li_2MnO_3 and $L_{1.2}Ni_{0.2}Mn_{0.6}O_2$, indicating that the formation of Li_2O is only observed with compositions exhibiting oxygen activation. The higher range from 3000 to 4000 cm^{-1} was taken for the initial, fully charged and discharged state (see Figure S2) in order to observe if there were any indications of water contamination before electrochemical measurements related to the formation of $LiOH{\cdot}H_2O$ or hydrolysis occurring: no OH band was observed.

The signals for several of the bands corresponding to the individual surface species, although discernible, are generally weak, similar to the SERS study of oxygen reaction in nonaqueous electrolyte on a Au electrode.[13] To increase the signal from the different surface formations, *in situ* SERS for the $Li_{1.2}Ni_{0.2}Mn_{0.6}O_2$ and $LiNi_{0.5}Mn_{0.5}O_2$ compositions were repeated under the same conditions with only the laser power increased from 1 to 10 mW and then compared. In Figure 4, for both compositions, the bands corresponding to the surface formations have increased dramatically. The Li_2CO_3 bands are clearly seen beginning at 4.0 V as well as the C−O stretching band at 957 cm^{-1} upon charging. Li_2CO_3 bands decrease considerably at 4.8 V corresponding well with the 1 mW condition. In Figure 4a, the Li_2O band for $Li_{1.2}Ni_{0.2}Mn_{0.6}O_2$ can be clearly seen as the evolution follows the same trend as the 1 mW condition. In Figure 4b, no Li_2O band was observed for $LiNi_{0.5}Mn_{0.5}O_2$. Compared to the 1 mW condition, the band at 834 cm^{-1} was not observed for the $Li_{1.2}Ni_{0.2}Mn_{0.6}O_2$ composition during charging at 10 mW. This may be due to the increased probability of laser-induced degradation caused by the increased power, which has a much greater effect on organic species. Similar to the LLNMO taken at 1 mW, the voltage was held for several minutes to observe the evolution over time for the LLNMO at 10 mW laser power (see Figure S3). The Li_2O band increases upon reaching the

dx.doi.org/10.1021/ja410137s | J. Am. Chem. Soc. 2014, 136, 999−1007

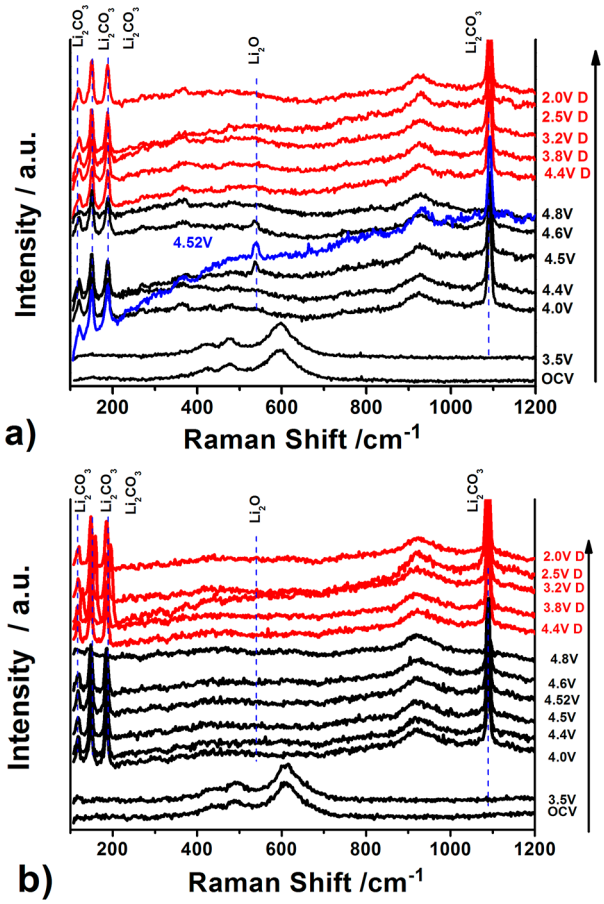

Figure 4. *In* situ SERS at 10 mW laser power for (a) $Li_{1.2}Ni_{0.2}Mn_{0.6}O_2$ and (b) $LiNi_{0.5}Mn_{0.5}O_2$.

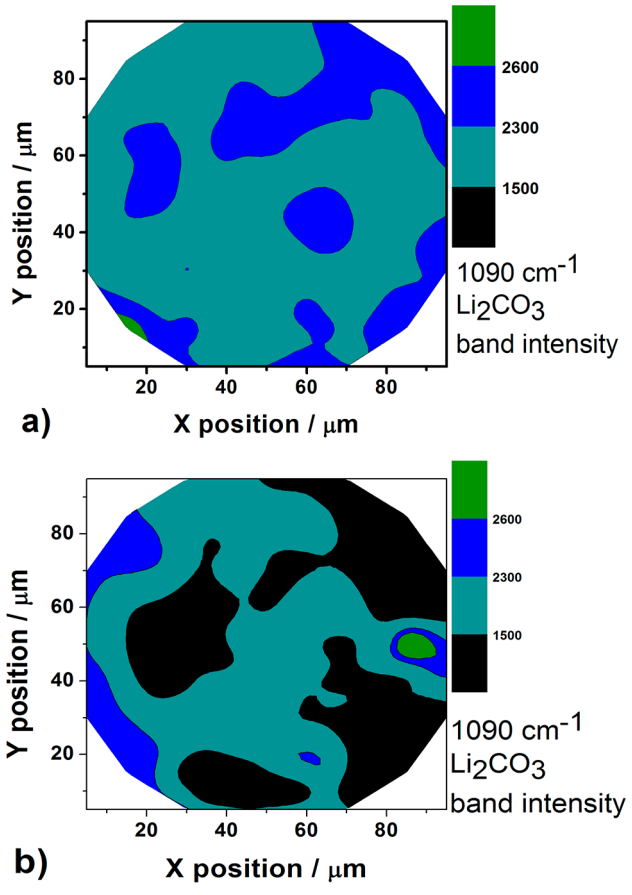

Figure 5. Raman mapping of (a) $Li_{1.2}Ni_{0.2}Mn_{0.6}O_2$ and (b) $LiNi_{0.5}Mn_{0.5}O_2$ after discharge to 2.0 V showing the 1090 cm^{-1} Li_2CO_3 band intensity.

plateau region and gradually decreases upon increasing the voltage.

While the enhancements of Li_2O for 1 mW and 10 mW were similar, Li_2CO_3 showed a more dramatic enhancement when run under 10 mW laser power. Li_2CO_3 and Li_2O standards run under both laser powers showed that this intensity increase is related to the adjustment of the laser power (see Figure S4). It should also be mentioned that without the use of a SERS probe or substrate, the different surface formations would generally not be observable under normal Raman conditions, especially under *in situ* conditions, regardless of any adjustment to the laser's power (see Figure S5). Furthermore, laser-induced changes may occur if the laser power is increased.[16]

Observation of Li_2CO_3 surface coverage was done over a 100 × 100 μm area of the electrode after discharging to 2.0 V by mapping the 1090 cm^{-1} band. Figure 5a,b depicts $Li_{1.2}Ni_{0.2}Mn_{0.6}O_2$ and $LiNi_{0.5}Mn_{0.5}O_2$, respectively. Examples of the spectra for both of the electrodes can be found in the Supporting Information (see Figure S6). Intensities below 1500 (black) counts are areas considered background. For $Li_{1.2}Ni_{0.2}Mn_{0.6}O_2$, full coverage of Li_2CO_3 is observed within the area, but several small areas show much higher intensities where the population of Li_2CO_3 may be denser. The area coverage is similar to observations under an optical microscope done over a larger area where the formation of white particles were observed.[11]

In comparison, $LiNi_{0.5}Mn_{0.5}O_2$ shows large areas where the signal drops below the background (black areas). The higher coverage of Li_2CO_3 on the oxygen activating material agrees well with previous studies showing high amounts of Li_2CO_3 after discharge.[11,12]

DISCUSSION

For the Li-rich cathode material, the charge compensation mechanism generally starts by the compensation of the $Ni^{2+/4+}$ redox couple where ~0.4 Li^+ would be extracted. This would give a corresponding theoretical capacity of 126 mAh/g represented by reaction (1) in Table 1 where the potential

Table 1. Different Reactions Occurring during Charging for $Li_{1.2}Ni_{0.2}Mn_{0.6}O_2$ up to 4.8 V

	reactions	E (V)
1	$Li_{1.2}Ni(II)_{0.2}Mn(IV)_{0.6}O\ (-II)_2 \leftrightarrow Li_{1.2-0.2x}Ni(II + x)_{0.2}Mn(IV)_{0.6}O_2(-II) + 0.2Li^+ + 0.2e^-$ $(x \leq 2)$ ($Ni^{2+/4+}$redox couple)	≤4.4
2	$Li_{0.8}Ni(IV)_{0.2}Mn(IV)_{0.6}O(-II)_2 \leftrightarrow Li_{0.8-2\delta}Ni(IV)_{0.2}Mn(IV)_{0.6}O(-II + \delta)_2 + 2\delta Li^+ + 2\delta e^-$ ($O^{2-/-}$ redox couple)	4.4 ≤ E ≤ 4.8
3	$Li_{0.8}Ni(IV)_{0.2}Mn(IV)_{0.6}O(-II)_2 \rightarrow Li_{0.8-2\delta}Ni(IV)_{0.2}Mn(IV)_{0.6}O(-II)_{2-2\delta} + \delta Li_2O$	4.4 ≤ E ≤ 4.8
4	$Li_{0.8-2\delta}Ni(IV)_{0.2}Mn(IV)_{0.6}O(-II+\delta)_2$ + solvents → $Li_{0.8-2\delta}Ni(IV)_{0.2}Mn(IV)_{0.6}O(-II + \delta)_2 + CO\uparrow + CO_2\uparrow$ + other products + γ H^++ γe^- (catalytic reaction)	4.4 ≤ E ≤ 4.8
5	$Li_{0.8-2\delta}Ni(IV)_{0.2}Mn(IV)_{0.6}O(-II + \delta)_2 \rightarrow Li_{0.8-2\delta}Ni(IV)_{0.2}Mn(IV)_{0.6}O(-II)_{2-\delta} + \delta/2O_2\uparrow$	4.4 ≤ E ≤ 4.8
6	$Li_2O + 2H^+ \rightarrow 2Li^+ + H_2O$	4.4 ≤ E ≤ 4.8
7	$Li_2O + CO_2 \rightarrow Li_2CO_3$	4.4 ≤ E ≤ 4.8

dx.doi.org/10.1021/ja410137s | J. Am. Chem. Soc. 2014, 136, 999−1007

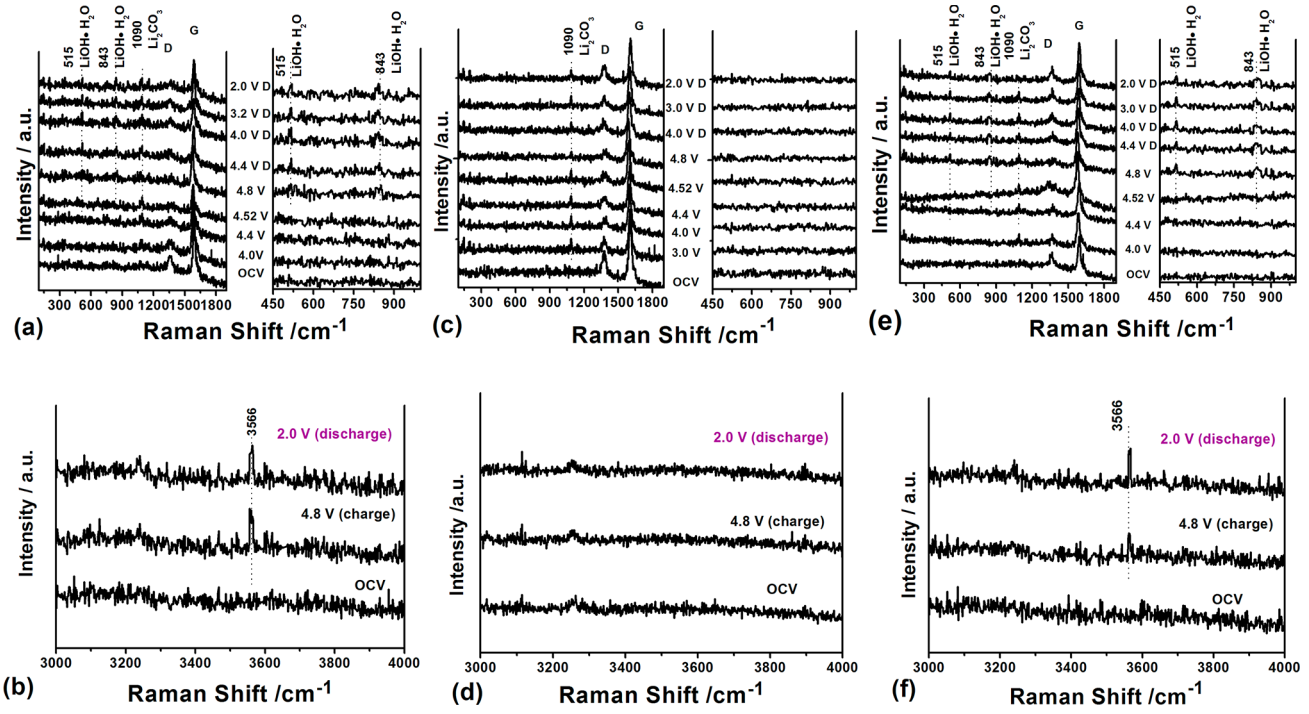

Figure 6. *In situ* SERS spectra of MCMB of the Li_2MnO_3/MCMB battery for the (a) lower and (b) higher frequency range; $LiNi_{0.5}Mn_{0.5}O_2$ /MCMB battery for the (c) lower and (d) higher frequency range; and $Li_{1.2}Ni_{0.2}Mn_{0.6}O_2$/MCMB battery for the (e) lower and (f) higher frequency range. D indicates discharge for the lower frequency.

range specifies when the specific reaction will likely occur. The possibility of Mn participation has been explored where Mn^{4+} is reduced after the first discharge (at least partially) to Mn^{3+} which can participate in subsequent cycles.[11,29,40,41] Recently, several authors have focused on the participation of oxygen in the charging compensation beyond the $Ni^{2+/4+}$ redox.[27,41−44] Fell et al.[44] have shown experimentally through Rietveld refinement of synchrotron XRD and EELS of the same material, the presence of oxygen vacancies and possible oxygen activation within the bulk structure. They explored the role of oxygen and suggested that the formation of oxygen vacancies associated with Mn reduction leads to the generation of Li_2O_2 (via a superoxide) which reacts to form Li_2O.[41]

Koga et al.,[43] similarly proposed the activation and participation of oxygen between two phases within $Li_{1.2}Mn_{0.54}Co_{0.13}Ni_{0.13}O_2$ in the charging mechanism through XRD analysis. Sathiya et al.[27] showed direct evidence of oxygen participation through XPS analysis at different charged states of $Li_2Ru_{0.5}Mn_{0.5}O_3$ where lattice oxygen was partially converted from O^{2-} to O^- after the oxygen plateau. Based on these previous studies of the anion redox participation, several possible reactions may take place and lead to the formation of Li_2O as well as other related products. When the oxidation of Ni^{2+} has reached an oxidation state of 4+, oxygen activation occurs following electrochemical reaction (2). Although this process is reversible, the activation of oxygen leaves the LLNMO highly reactive and highly unstable, i.e., similar to a catalyst or reactive species. After the occurrence of reaction (2), reactions (3−5) can occur with direct interaction of the LLNMO material where electrochemical reaction (3) forms Li_2O, which can be considered irreversible. It has been proposed that Li_2O may form from LiO_2 or Li_2O_2, but neither LiO_2 nor Li_2O_2 were observed during the SERS measurements.[41] Reaction (4) is the LLNMO oxygen activated material reacting with the electrolyte solvents to form the electrolyte degradation products as well as a proton (H^+) and several gases such as CO_2 and CO through an irreversible catalytic reaction. Reaction (5), which is also irreversible, would be the third reaction that may also occur where O_2 gas would be released to stabilize the LLNMO material.

Regarding the evolution of the different gases, previous results have shown gas evolution during charging and specifically within the oxygen plateau region.[12,35,45−47] Hong et al.[12] showed, using differential electrochemical mass spectroscopy (DEMS), the formation of CO, CO_2, and O_2. Interestingly, their results showed that gas formation occurred from the middle toward the end of the plateau, reaching its peak at the end of charge. Specifically, O_2 gas evolution did not occur until the end of charge (4.8 V), while CO and CO_2 showed small accumulations in the middle of the plateau (~4.55 V), increasing dramatically at the end of charge. Gas evolution toward the end of charging rather than the beginning of the plateau has also been observed by other workers.[45−47] This suggests that reactions (4) and (5) are more significantly closer to the end of charging, while reaction (3) proceeds at the beginning of the plateau region. However, it cannot be ruled out that O_2 may have some degree of solubility into the electrolyte, be consumed by the oxidation of lithium-organic compounds, or take part in forming Li_2O.[24] Thus reaction (5) may occur during the plateau where O_2 evolution only is observed near the end-of-charge upon completing its reaction or exceeding the solubility limit of the electrolyte. At the beginning of discharge the generation of CO and CO_2 declines rapidly, possibly reacting to form Li_2CO_3 and other products. Interestingly, CO and CO_2 evolution has been shown to continue, at a reduced rate, after the first cycle, while O_2 evolution ceases after the first cycle.[38,40] It is speculated that reaction (4) may continue to occur after the first cycle causing

dx.doi.org/10.1021/ja410137s | J. Am. Chem. Soc. 2014, 136, 999−1007

Scheme 1. Proposed Surface Reaction Mechanism of $Li[Ni_xLi_{(1-2x)/3}Mn_{(2-x)/3}]O_2$ for Oxygen Activating Members during Charging and Discharging (top) and Charging/Discharging Curve Showing the Different Process (bottom)

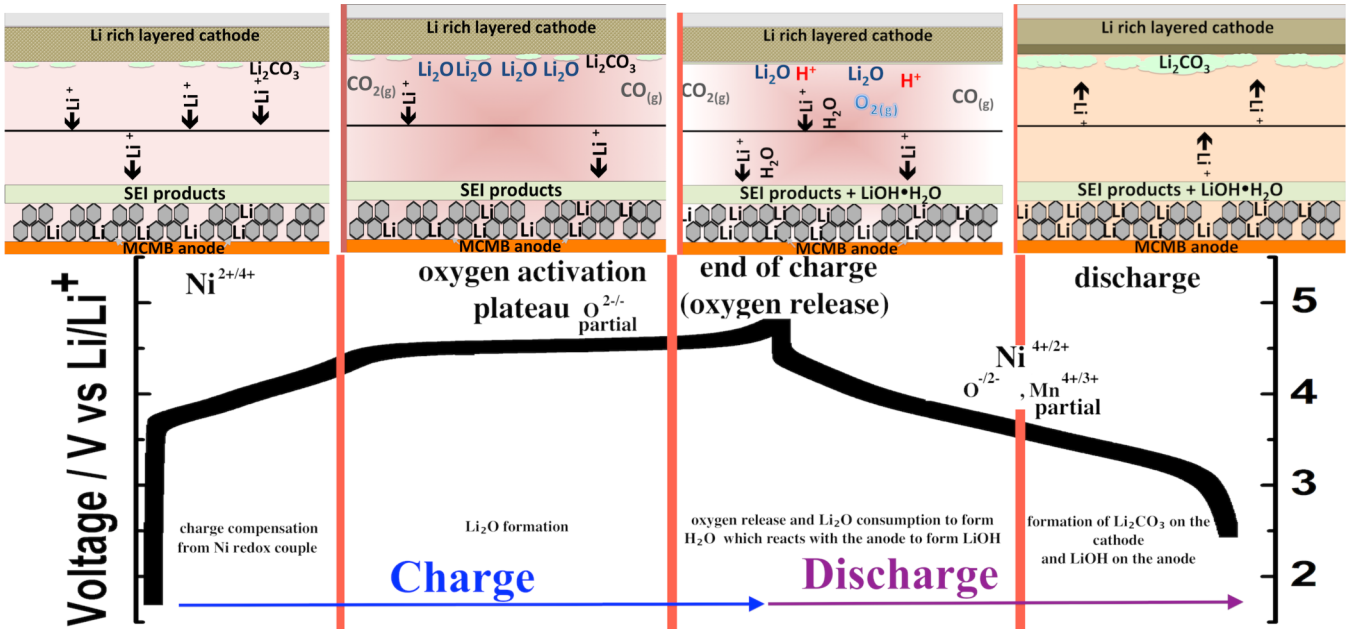

continuous electrolyte decomposition leading to capacity fade, due to exhaustion of the electrolyte supply.[36]

As mentioned above, during the oxygen-activating plateau, Li_2O is formed and then subsequently consumed toward the end of the plateau. The consumption of Li_2O would likely occur via reaction (6), i.e., with H^+ to form H_2O and/or (7) reacting with CO_2 to form Li_2CO_3.

It should be noted that reactions (6) and (7) are not potential dependent but are chemical reactions dependent on the supply of Li_2O. It is possible that the generation of Li_2O from the electrochemical reaction and its consumption in reactions (6) and (7) take place simultaneously in the plateau region at a similar rate. When the end-of-plateau is reached and the potential further increases, the rate of Li_2O generation declines and is much lower than the rate of reaction (6) and (7). The presence of H_2O has previously been reported to lead to Mn dissolution and surface degradation and the dissolution of Mn.[12] In the presence of H_2O, the lithium salt may undergo reactions with $LiPF_6$[12] and other electrolyte components where it can form HF that is able to dissolve the material's surface. However, no indication of direct H_2O interaction on the cathode surface was observed during the first cycle *in situ* studies for the three LLNMO materials. The other possibility is the reaction of H_2O with the intercalated anode to form LiOH. Considering the high level of precipitation of Li_2CO_3 onto the cathode's surface at the discharged state, the interaction of Li_2O with H^+ and subsequent formation of LiOH may alter the electrolyte solution from acidic to more neutral. This would favor Li_2CO_3 precipitation by providing a favorable environment for Li_2CO_3 to form on the surface of the cathode where the different gases, e.g., CO_2, may dissolve into the electrolyte and react to form Li_2CO_3.

In order to confirm changes within the electrolyte solution, *in situ* SERS was run to observe formation of $LiOH{\cdot}H_2O$ in a full cell configuration, which consisted of the LLNMO material with a small hole applied to the electrode and the $Au@SiO_2$ NP applied to the MCMB anode where the MCMB anode was the electrode probed. Figure 6a,b shows the Raman spectra evolution of the MCMB anode in the Li_2MnO_3/MCMB full cell during charging (insertion) and discharging (extraction), for the low- and high-frequency ranges, respectively. The evolution of the D (disorder-induced A_{1g} band) and G (C−C stretching mode, E_{2g2}) band follows the evolution of Li insertion and extraction seen in other disordered graphite anodes[48] where the D band intensity slightly decreases (I_G/I_D increases) and the G band moves from 1590 cm^{-1} toward the lower frequency during insertion before reaching the graphite dilute stage 1 and back to higher frequency during extraction.[48]

For the surface formation, at 4.0 V the peak at 1090 cm^{-1} corresponding to Li_2CO_3 formation can be observed and is present even after discharging to 2.0 V. Starting at the end of charging (4.8 V), two new bands appear at 515 and 843 cm^{-1} that correspond to $LiOH{\cdot}H_2O$ which remains after discharged to 2.0 V. The higher frequency range also shows the OH stretching band at 3566 cm^{-1} at the end of the charged (4.8 V) state and the discharged (2.0 V) state. Figure 6c,d shows the Raman spectra for the MCMB anode of the $LiNi_{0.5}Mn_{0.5}O_2$/MCMB full cell (non-Li_2O forming material) for the lower and higher frequency ranges, respectively. The graphite bands during lithium insertion and extraction in the $LiNi_{0.5}Mn_{0.5}O_2$/MCMB full cell show similar evolution to that of the Li_2MnO_3/MCMB full cell. However, throughout the charging and discharging process, only the band corresponding to Li_2CO_3 (1090 cm^{-1}) is present, and no indication of LiOH was found in the low or high frequency ranges.

Finally, to confirm the formation of LiOH occurring on the Li_2O forming materials series, the Raman measurements for the $Li_{1.2}Ni_{0.2}Mn_{0.6}O_2$/MCMB full cell were performed, as shown in Figure 6e,f. The evolution of the graphite bands is similar to those previously described, except for a slight distortion of the spectra during charging at 4.52 V. Similar to the Li_2MnO_3/MCMB full cell, LiOH bands at low and high frequencies can be seen at the end of charge that remain after discharging to 2.0 V. This confirms the formation of LiOH, by the interaction of H_2O formed from Li_2O.

dx.doi.org/10.1021/ja410137s | J. Am. Chem. Soc. 2014, 136, 999−1007

To further confirm the changes to the electrolyte system, favoring precipitation of the surface deposits, the electrolyte pH was investigated using $Li_{1.2}Ni_{0.2}Mn_{0.6}O_2$ batteries run in an Ar-filled glovebox and stopped at different potentials. The batteries were then opened, and the pH of the electrolyte was quickly measured by litmus paper (see Figure S9).

When charged before reaching the plateau (4.4 V) the solution changes to a more acidic environment than the solution at OCV and maintains this environment when discharged to 2.5 V. When charged to 4.8 V (after the plateau has finished) and discharged to 2.5 V, the solution changes from an acidic environment before and during the plateau to a more neutral environment after discharged. This confirms that the presence of Li_2O evolution will change the electrolyte solution environment from acidic to more neutral, while in the absence of it there is not such a dramatic change. Lee et al.[49] showed that $LiCoO_2$ and $LiCoPO_4$ under oxygen evolution reaction conditions, at varying pH values, the cathode's surface will either be amorphous (pH = 13) or spinel (pH = 7). Previous reports[7,29] have shown the conversion of a layered to a spinel surface when continuously cycled, and several workers have shown HRTEM images of the growth of an amorphous layer.[12,50] This correlates well with the changes of the surface of the material with the electrolyte condition.

Scheme 1 illustrates the proposed surface reaction mechanism for LLNMO that occurs during charging and discharging for oxygen activating members, based on the results of the previous studies mentioned in the article and the surface reactions observed for the cathode and anode sides during the *in situ* SERS studies. Before the plateau the formation of the SEI on the anode side occurs with a limited formation of Li_2CO_3 on the cathode side from the interaction with the electrolyte where the charge compensation follows the $Ni^{2+/4+}$ redox couple. During the plateau, activation of oxygen occurs as well as Li_2O formation. Electrolyte degradation may also occur, forming gases such as CO and CO_2. Toward the end of the plateau, the unstable and catalyst-like LLNMO material causes the release of O_2 gas as well as readily reacting with the electrolyte to form CO, CO_2, and protons (H^+) via a catalytic reaction. Li_2O will react with the proton (H^+) to form Li^+ and H_2O which solvates and migrates to the anode side forming $LiOH{\cdot}H_2O$ at the end of charging. The discharge compensation mechanism is thought to be a combination of the $Ni^{2+/4+}$ redox couple, oxygen anion redox couple, and the partial participation of $Mn^{3+/4+}$ that continually grows with increasing cycles. It should be noted, although changes have been observed, the role of Mn in the charging compensation mechanism is still not clear but may be related to bulk stabilization. Toward the end of the discharging process, the reaction of H^+ and formation of LiOH leads to the solution changes from an acidic to a more neutral environment leading to highly cathodic Li_2CO_3 precipitation that leads to a diminished performance.

In summary, by using *in situ* SERS to observe surface phenomena for both the anode and the cathode, we have provided direct evidence of Li_2O formation on lithium-rich cathode materials and the formation of $LiOH{\cdot}H_2O$ on the anode. The consequences of this formation and a comprehensive mechanism were discussed considering oxygen anion redox charge compensation. Upon reaching the plateau at ~4.5 V where oxygen is activated, the formation of Li_2O and its subsequent reactions lead to the hydrolysis of the electrolyte, and changes within the solution lead to the formation of Li_2CO_3 and other related products when discharged. Our results suggest that consideration of both the cathode and anode is crucial to elucidating the nature of the reactions occurring within the entire battery system to improve its performance. Furthermore focusing on not only surface coatings to improve the stability but also on the electrolyte should provide a route to improve the performance of these materials.

■ ASSOCIATED CONTENT

Supporting Information

Raman spectra for $Li_{1.2}Ni_{0.2}Mn_{0.6}O_2$ cathode and MCMB anode, *in situ* SERS spectra and normal Raman comparison, SERS spectra running at constant current charging protocol, Raman spectra for mapping, and images of pH measurements. This material is available free of charge via the Internet at http://pubs.acs.org.

■ AUTHOR INFORMATION

Corresponding Author

bjh@mail.ntust.edu.tw

Notes

The authors declare no competing financial interest.

■ ACKNOWLEDGMENTS

Financial support from the National Science Council (NSC) grant nos. (101-3113-E-011-002, 101-2923-E-011-001-MY3, 100-2221-E-011-105-MY3), the Ministry of Economic Affairs (MOEA) (101-EC-17-A-08-S1-183), and the Top University Projects of Ministry of Education (MOE) (100H451401) as well as the facilities support from the National Taiwan University of Science and Technology (NTUST) are acknowledged. Damien S. Clark for his insightful discussions and suggestions.

■ REFERENCES

(1) Lu, Z.; MacNeil, D. D.; Dahn, J. R. *Electrochem. Solid-State Lett.* **2001**, *4*, A191.
(2) Johnson, C. S.; Kim, J. S.; Lefief, C.; Li, N.; Vaughey, J. T.; Thackeray, M. M. *Electrochem. Commun.* **2004**, *6*, 1085.
(3) Thackeray, M. M.; Johnson, C. S.; Vaughey, J. T. *J. Mater. Chem.* **2005**, *15*, 2257.
(4) Hwang, B. J.; Wang, C. J.; Chen, C. H.; Tsai, Y. W.; Venkateswarlu, M. *J. Power Sources* **2005**, *146*, 658.
(5) Lu, Z.; Dahn, J. R. *J. Electrochem. Soc.* **2002**, *149*, A815.
(6) Jarvis, K. A.; Deng, Z.; Allard, L. F.; Manthiram, A.; Ferreira, P. J. *Chem. Mater.* **2011**, *23*, 3614.
(7) Gu, M.; Belharouak, I.; Zheng, J.; Wu, H.; Xiao, J.; Genc, A.; Amine, K.; Thevuthasan, S.; Baer, D. R.; Zhang, J.-G.; Browning, N. D.; Liu, J.; Wang, C. *ACS Nano* **2012**, *7*, 760.
(8) Hu, M.; Pang, X.; Zhou, Z. *J. Power Sources* **2013**, *237*, 229.
(9) Ohzuku, T.; Nagayama, M.; Tsuji, K.; Ariyoshi, K. *J. Mater. Chem.* **2011**, *21*, 10179.
(10) Thackeray, M. M.; Kang, S.-H.; Johnson, C. S.; Vaughey, J. T.; Benedek, R.; Hackney, S. A. *J. Mater. Chem.* **2007**, *17*, 3112.
(11) Yabuuchi, N.; Yoshii, K.; Myung, S.-T.; Nakai, I.; Komaba, S. *J. Am. Chem. Soc.* **2011**, *133*, 4404.
(12) Hong, J.; Lim, H.-D.; Lee, M.; Kim, S.-W.; Kim, H.; Oh, S.-T.; Chung, G.-C.; Kang, K. *Chem. Mater.* **2012**, *24*, 2692.
(13) Peng, Z.; Freunberger, S. A.; Hardwick, L. J.; Chen, Y.; Giordani, V.; Barde, F.; Novak, P.; Graham, D.; Tarascon, J. M.; Bruce, P. G. *Angew. Chem., Int. Ed. Engl.* **2011**, *50*, 6351.
(14) Li, J.-F.; Li, S.-B.; Anema, J. R.; Yang, Z.-L.; Huang, Y.-F.; Ding, Y.; Wu, Y.-F.; Zhou, X.-S.; Wu, D.-Y.; Ren, B.; Wang, Z.-L.; Tian, Z.-Q. *Appl. Spectrosc.* **2011**, *65*, 620.
(15) Yu, D. Y. W.; Yanagida, K. *J. Electrochem. Soc.* **2011**, *158*, A1015.

(16) Burba, C. M.; Palmer, J. M.; Holinsworth, B. S. *J. Raman Spectrosc.* **2009**, *40*, 225.
(17) Li, J. F.; Huang, Y. F.; Ding, Y.; Yang, Z. L.; Li, S. B.; Zhou, X. S.; Fan, F. R.; Zhang, W.; Zhou, Z. Y.; Wu, D. Y.; Ren, B.; Wang, Z. L.; Tian, Z. Q. *Nature* **2010**, *464*, 392.
(18) Thapa, A. K.; Saimen, K.; Ishihara, T. *Electrochem. Solid-State Lett.* **2010**, *13*, A165.
(19) Verma, P.; Maire, P.; Novák, P. *Electrochim. Acta* **2010**, *55*, 6332.
(20) Li, G.; Li, H.; Mo, Y.; Chen, L.; Huang, X. *J. Power Sources* **2002**, *104*, 190.
(21) Dedryvère, R.; Martinez, H.; Leroy, S.; Lemordant, D.; Bonhomme, F.; Biensan, P.; Gonbeau, D. *J. Power Sources* **2007**, *174*, 462.
(22) Matsui, M.; Dokko, K.; Kanamura, K. *J. Power Sources* **2008**, *177*, 184.
(23) Peng, Z.; Freunberger, S. A.; Chen, Y.; Bruce, P. G. *Science* **2012**, *337*, 563.
(24) Schroder, K. W.; Celio, H.; Webb, L. J.; Stevenson, K. J. *J. Phys. Chem. C* **2012**, *116*, 19737.
(25) Freunberger, S. A.; Chen, Y.; Peng, Z.; Griffin, J. M.; Hardwick, L. J.; Barde, F.; Novak, P.; Bruce, P. G. *J. Am. Chem. Soc.* **2011**, *133*, 8040.
(26) Paulsen, J. M.; Thomas, C. L.; Dahn, J. R. *J. Electrochem. Soc.* **2000**, *147*, 861.
(27) Sathiya, M.; Ramesha, K.; Rousse, G.; Foix, D.; Gonbeau, D.; Prakash, A. S.; Doublet, M. L.; Hemalatha, K.; Tarascon, J. M. *Chem. Mater.* **2013**, *25*, 1121.
(28) Gopukumar, S.; Chung, K. Y.; Kim, K. B. *Electrochim. Acta* **2004**, *49*, 803.
(29) Hy, S.; Su, W.-N.; Chen, J.-M.; Hwang, B.-J. *J. Phys. Chem. C* **2012**, *116*, 25242.
(30) Julien, C. M.; Massot, M. *Mater. Sci. Eng., B* **2003**, *100*, 69.
(31) Amalraj, S. F.; Sharon, D.; Talianker, M.; Julien, C. M.; Burlaka, L.; Lavi, R.; Zhecheva, E.; Markovsky, B.; Zinigrad, E.; Kovacheva, D.; Stoyanova, R.; Aurbach, D. *Electrochim. Acta* **2013**, *97*, 259.
(32) Tran, N.; Croguennec, L.; Ménétrier, M.; Weill, F.; Biensan, P.; Jordy, C.; Delmas, C. *Chem. Mater.* **2008**, *20*, 4815.
(33) Okazaki, S.; Ohtori, N.; Okada, I. *J. Chem. Phys.* **1989**, *91*, 5587.
(34) Larkin, P. *Infrared and Raman Spectroscopy: principles and spectral interpretation*; Elsevier, Inc.: Waltham, MA, 2011.
(35) Jiang, M.; Key, B.; Meng, Y. S.; Grey, C. P. *Chem. Mater.* **2009**, *21*, 2733.
(36) Black, R.; Oh, S. H.; Lee, J.-H.; Yim, T.; Adams, B.; Nazar, L. F. *J. Am. Chem. Soc.* **2012**, *134*, 2902.
(37) Hong, J.; Seo, D.-H.; Kim, S.-W.; Gwon, H.; Oh, S.-T.; Kang, K. *J. Mater. Chem.* **2010**, *20*, 10179.
(38) Singh, G.; West, W. C.; Soler, J.; Katiyar, R. S. *J. Power Sources* **2012**, *218*, 34.
(39) Yabuuchi, N.; Yoshii, K.; Myung, S. T.; Nakai, I.; Komaba, S. *J. Am. Chem. Soc.* **2011**, *133*, 4404.
(40) Ito, A.; Sato, Y.; Sanada, T.; Hatano, M.; Horie, H.; Ohsawa, Y. *J. Power Sources* **2011**, *196*, 6828.
(41) Carroll, K. J.; Qian, D.; Fell, C.; Calvin, S.; Veith, G. M.; Chi, M.; Baggetto, L.; Meng, Y. S. *Phys. Chem. Chem. Phys.* **2013**, *15*, 11128.
(42) Oishi, M.; Fujimoto, T.; Takanashi, Y.; Orikasa, Y.; Kawamura, A.; Ina, T.; Yamashige, H.; Takamatsu, D.; Sato, K.; Murayama, H.; Tanida, H.; Arai, H.; Ishii, H.; Yogi, C.; Watanabe, I.; Ohta, T.; Mineshige, A.; Uchimoto, Y.; Ogumi, Z. *J. Power Sources* **2013**, *222*, 45.
(43) Koga, H.; Croguennec, L.; Ménétrier, M.; Mannessiez, P.; Weill, F.; Delmas, C. *J. Power Sources* **2013**, *236*, 250.
(44) Fell, C. R.; Qian, D.; Carroll, K. J.; Chi, M.; Jones, J. L.; Meng, Y. S. *Chem. Mater.* **2013**, *25*, 1621.
(45) Lanz, P.; Sommer, H.; Schulz-Dobrick, M.; Novák, P. *Electrochim. Acta* **2013**, *93*, 114.
(46) La Mantia, F.; Rosciano, F.; Tran, N.; Novák, P. *J. Appl. Electrochem.* **2008**, *38*, 893.
(47) Armstrong, A. R.; Holzapfel, M.; Novák, P.; Johnson, C. S.; Kang, S.-H.; Thackeray, M. M.; Bruce, P. G. *J. Am. Chem. Soc.* **2006**, *128*, 8694.
(48) Hardwick, L.; Buqa, H.; Novak, P. *Solid State Ionics* **2006**, *177*, 2801.
(49) Lee, S. W.; Carlton, C.; Risch, M.; Surendranath, Y.; Chen, S.; Furutsuki, S.; Yamada, A.; Nocera, D. G.; Shao-Horn, Y. *J. Am. Chem. Soc.* **2012**, *134*, 16959.
(50) Xu, B.; Fell, C. R.; Chi, M.; Meng, Y. S. *Energy Environ. Sci.* **2011**, *4*, 2223.